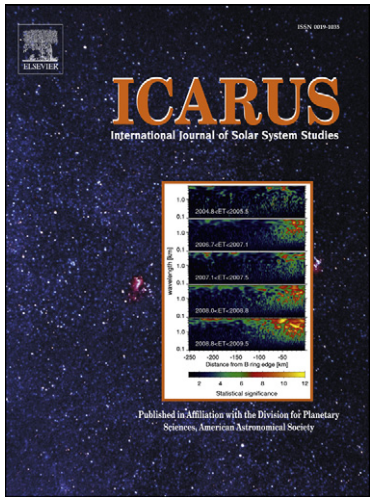

Oxygen nightglow emissions of Venus: Vertical distribution and collisional quenching

J.-C. Gérard, L. Soret, A. Migliorini, G. Piccioni

PII: S0019-1035(12)00473-3
DOI: http://dx.doi.org/10.1016/j.icarus.2012.11.019
Reference: YICAR 10460

To appear in: *Icarus*

Please cite this article as: Gérard, J.-C., Soret, L., Migliorini, A., Piccioni, G., Oxygen nightglow emissions of Venus: Vertical distribution and collisional quenching, *Icarus* (2012), doi: http://dx.doi.org/10.1016/j.icarus.2012.11.019

Oxygen nightglow emissions of Venus: Vertical distribution and collisional quenching

J.-C. Gérard, L. Soret

Laboratoire de Physique Atmosphérique et Planétaire
Université de Liège
Liège – Belgium

A. Migliorini, G. Piccioni
IAPS-INAF
Rome - Italy

Submitted for publication to Icarus

Revised, November 2012

Corresponding author:

Pr. J.-C. Gérard
Laboratoire de Physique Atmosphérique et Planétaire
Université de Liège – B5c
Allée du 6 août, 16 – Sart Tilman
B-4000 Liège (Belgium)

E-mail: jc.gerard@ulg.ac.be
Phone: 32-43669775
Fax: 32-43669711

Regular paper

32 pages
3 tables
3 figures

The three figures are intended to be published in color in the printed version of Icarus.

•

Abstract

We compare the altitude of three O_2 night airglow emissions observed at the limb of Venus by the VIRTIS spectral imager with the values predicted by a model accounting for the different radiative lifetimes and collisional deactivation of the upper O_2 states. The O and CO_2 density profiles are based on remote sensing observations from the Venus Express spacecraft. Effective production efficiencies of the involved O_2 metastable states and quenching coefficients by oxygen and carbon dioxide are adjusted to provide the best match with the measured emission limb profiles. We find values in general good agreement with earlier studies for the $c^1\Sigma^-_u$ state which gives rise to the Herzberg II bands. In particular, we confirm the low net yield of the c state production and the importance of its deactivation by CO_2, for which we derive a quenching coefficient of $3x10^{-16}$ cm^{-3} s^{-1}. The ~4.5 km higher altitude of the Chamberlain band emission also recently detected by VIRTIS and the ratio of the Herzberg II/Chamberlain bands observed with Venera are well reproduced. To reach agreement, we use a 12% yield for the $A'^3\Delta_u$ production following O atom association and quenching coefficients by O and CO_2 of $1.3x10^{-11}$ cm^{-3} s^{-1} and $4.5x10^{-13}$ cm^{-3} s^{-1} respectively. We conclude that the different peak altitudes of the IR Atmospheric, Herzberg II and the Chamberlain bands reflect the relative importance of radiative relaxation and collisional quenching by O and CO_2.

1. Introduction

The oxygen nightglow has been used as a tool to probe the Venus global dynamics and composition of the night side of the planet. Through its comparison with the airglow of the Earth and Mars, it has also been a valuable source of information on the production and collisional deactivation of the O_2 metastable states when two oxygen atoms recombine in a three-body reaction. Interestingly, in spite of considerable efforts devoted for decades to quantify the recombination products and their subsequent fate in terrestrial planetary atmospheres, uncertainties remain to get a consistent quantitative picture of the processes involved. The set of observations collected with the VIRTIS instrument on board Venus Express has recently provided information on both the intensity and the vertical distribution of several O_2 nightglow emissions with unprecedented accuracy. In this study, we take advantage of new observations of the Venus O_2 visible nightglow reported in a companion paper (Migliorini et al., submitted to Icarus) to compare the characteristics of three O_2 emissions with the modeled distributions expected from the atomic oxygen and the CO_2 vertical density distributions derived from remote sensing observations performed from Venus Express.

The source of the O_2 nightglow is the recombination process with a third body M (mainly CO_2, CO or O):

$$O + O + M \rightarrow O_2^* + M \qquad (1)$$

whose excess energy is 5.12 eV if the O_2 molecule is formed in the ground state X(v=0) level. Consequently, the oxygen molecule may be produced in several electronic excited

state denoted here O_2*. As the molecule relaxes radiatively, photons are emitted in several band systems. Some of these have been observed in the Earth, Mars and Venus nightside airglow. The main transitions associated to these states are the A $^3\sum \rightarrow$X $^3\sum$ Herzberg I bands, the A' $^3\Delta \rightarrow$ a $^1\Delta$ Chamberlain bands, the a $^1\Delta \rightarrow$ X $^3\sum$ Atmospheric IR bands, the c $^1\sum \rightarrow$ X $^3\sum$ Herzberg II bands, the b $^1\sum \rightarrow$ X $^3\sum$ Atmospheric bands, and the b $^1\sum \rightarrow$ a $^1\Delta$ Noxon bands. The relative intensity of these emissions in the atmospheres of the three terrestrial planets has been discussed in several studies (Slanger et al., 2006; García-Muñoz et al., 2009; Krasnopolsky, 2011). The relative concentrations of CO_2, N_2 and O in the upper mesosphere of Venus and the Earth control the relative intensity of the nightglow emissions arising from the various O_2 metastable states (Slanger and Copeland, 2003; Krasnoplosky, 2011).

The O_2 a$^1\Delta$-X$^3\sum$ (0-0) Infrared Atmospheric band emission at 1.27 μm (IR Atm) has been extensively studied during the recent years. Following its detection by Connes et al. (1979), spatially resolved ground-based observations (Allen et al., 1992; Crisp et al., 1996; Lellouch et al., 1997; Ohtsuki et al., 2008; Bailey et al., 2008) have shown that the spatial distribution of the O_2 Atmospheric infrared airglow exhibits spatial and time variations on time scales of about one Earth day. Images indicate that these rapidly changing bright areas are observed most frequently at low latitudes between midnight and 03:00 local time. Drossart et al. (2007) reported the first limb observation of the 1.27 m emission on Venus and showed that the O_2 (a$^1\Delta$) peak at the limb is located near 96 km, a value consistent with excitation by three-body recombination of oxygen atoms. Gérard et al. (2008) analyzed the statistical distribution of the O_2 (a$^1\Delta$) airglow using both nadir and limb viewing geometries. They found that limb profiles observed at northern mid-latitudes exhibit large intensity variations over short time periods. They also showed that the limb profiles compare favorably with those obtained with a one-

dimensional chemical-diffusive model. Piccioni et al. (2009) and Gérard et al. (2009a) illustrated the variability and the complexity of the observed airglow limb profiles. The altitude, the brightness and the width of the emission peak vary with latitude. The altitude of maximum emission at the limb varies between 90 and 103 km, with a mean value of 96±2 km and the mean peak intensity along the line of sight is 28±23 MR (Gérard et al., 2010). As was shown by Gérard et al. (2009a), the O_2(a-X) airglow distribution may be used to infer the oxygen density distribution at different locations using the Abel inversion. They also found that the altitude of the airglow emission exhibits altitude variations as large as 10 km over short latitudinal distances. Additionally, Gérard et al. (2009b) demonstrated that the ultraviolet nitric oxide emitted near 115 km and the O_2 IR atmospheric bands near 96 km emissions are spatially uncorrelated. Soret et al. (2012) analyzed the full set of VIRTIS-M limb profiles at 1.27 μm to derive the three-dimensional distribution of O atoms in the mesosphere-thermosphere transition region. They found that the peak altitude of the O_2 ($a^1\Delta$) emission statistically increases from 94 km at the antisolar point to 99 km near the terminator, with a mean limb intensity over the northern nightside hemisphere of 27.5 MR at 96.2 km and a global mean nadir brightness of 500 kR. Following deconvolution and Abel inversion of each limb profile, the mean altitude of maximum volume emission rate was found at 99 km.

The Herzberg II (HzII) system was first observed with the spectrometers on board Venera 9 and 10 spacecraft by Krasnopolsky (1983). They found that the vertical intensity of the Herzberg II bands varied from 2 to 3 kR, with the highest values located near 00:00-01:00 LT. Observations with the spacecraft star tracker on board the Pioneer Venus confirmed the presence of the O_2 Herzberg II emission (Bougher and Borucki, 1994). The highest intensities were observed at low latitudes (3.6 kR vertical

brightness) and only weak local time variations were seen both in the Venera 9-10 and the Pioneer Venus nightglow. The presence of several bands of the weaker (0-v'') progression of the A' $^3\Delta \rightarrow$ a $^1\Delta$ Chamberlain (Ch) system was also identified in the Venera spectra by Slanger and Black (1978).

The Venus Express spacecraft was inserted into an elliptical 24-hour period orbit around Venus on April 11, 2006. It carried a suite of seven experiments designed to study Venus' atmosphere and plasma environment. One of them, the Visible and Infrared Thermal Imaging Spectrometer (VIRTIS) allows to acquire simultaneous spectra in the visible (0.28-1.1 μm) and infrared spectral ranges (1-5 μm) (Piccioni et al., in press). It can be operated both in nadir and limb observing modes, depending on the spacecraft position along its orbit. Among other objectives, nadir observations are used to investigate the distribution with latitude and longitude of selected airglow emissions, while the limb observations are best suited to study the altitude distribution of the emissions. García-Muñoz et al. (2009) carried out a first detailed study of the O_2 nightglow in the visible range using VIRTIS limb observations. They identified the (0-v'') Herzberg II bands with v''=6-11, exhibiting on the average a maximum emission at 95±1 km and a total c $\rightarrow$ X system intensity of 128 kR. They also suggested the presence of the Chamberlain bands, but no quantitative analysis was conducted. They compared these observations with a one-dimensional calculation where the c state is quenched by CO_2 and O and concluded that the net production of the c(0) state is on the order of 1-2%.

A recent campaign of VIRTIS observations in the limb-tracking mode allowed a new detection of the O_2 nightglow emissions in the visible spectral range (Migliorini et al., submitted to Icarus). About 8700 spectra, acquired in the period from March 4, 2007 to July 18, 2011, were averaged in order to obtain a mean spectrum in the altitude region 90-120 km. The spectrum is dominated by the presence of the Herzberg II c $^1\sum \rightarrow$ X $^3\sum$

system, from which they were able to clearly identify 8 bands, ranging from (0-6) to (0-13) bands. The authors discussed the statistical behavior of the sum of the most intense bands including the (0-7) to the (0-11) bands. However, they indicate that the full (0-v'') progression was not always observable in the dataset. This fact does not affect the peak altitude as it was previously verified that, as expected, each single band peaks at close altitudes. However, this affects the intensity, which is underestimated in those cases when some of the bands are not observed. Migliorini et al. (submitted to Icarus) only reported the intensity of (0-v'') progression for those data when the set of v''= 7 to 11 bands was detected. The intensity of the sum of the 0-7 to 0-11 bands was found to vary from 84 to 116 kR at the airglow peak. The average altitude of the maximum of all analyzed limb profiles was 95.5±1.6 km, in close agreement with the value of 95±1 km determined by García-Muñoz et al. (2009) from their average VIRTIS limb spectrum.

Three bands belonging the (0-v'') progression of the Chamberlain A' $^3\Delta \rightarrow a\ ^1\Delta$ system were also occasionally observed at the limb (Migliorini et al., submitted to Icarus). They are centered at 560 nm, 605 nm, and 657 nm, corresponding to the (0-6), (0-7), and (0-8) bands respectively. However, due to a lower efficiency above 650 nm of the VIRTIS grating, it was only possible to investigate the intensity and the peak altitude of the (0-6) and (0-7) bands. The two bands peak at about 100 km, that is 5 km higher than the Herzberg II bands. The measured relative intensity of these two bands is variable, a consequence of the difficulty to separate the Chamberlain bands from the adjacent Herzberg emission and the underlying noise. However, the (0-7)/(0-6) ratio was found to be 1.05 in one case and 1.27 in another case. These ratios are in satisfactory agreement with the theoretical value of 1.28 based on transition probabilities, considering the signal to noise limitations.

2. VIRTIS observations of the O_2 nightglow emissions

In brief, our methodology is as follows. We first summarize the peak altitude and the intensity ratio observations and determine the average characteristics of the O_2 airglow layers that will be modeled in the next section. For comparison with the airglow characteristics expected from a one-dimensional model, we then present the expression used to calculate the volume emission rate of the three band systems. We review the values initially adopted for the effective production efficiency of the excited states, the radiative lifetimes and the quenching coefficients by CO_2 and O atoms. The values of these coefficients are based on recent studies synthetizing the characteristics of the O_2 airglow on the three terrestrial planets. They will be modified as needed to fit the observational constraints provided by the Venera and the VIRTIS observations. We then describe the mean nightside vertical distribution of carbon dioxide and atomic oxygen used to calculate the vertical distribution of the volume emission rate (VER) and the limb profiles of the O_2 airglow. These density profiles are based on Venus Express observations made during the same time period as the airglow measurements reported in this study. We finally compare our best match with the O_2 airglow observations and draw conclusions concerning the set of excitation and quenching model parameters providing the best agreement with observations.

Table 1 summarizes the available information concerning the averaged altitude and maximum intensity of the nightglow limb profiles derived from VIRTIS observations. The levels of accuracy and confidence in the values are drastically different between the three emissions. The 1.27 μm (0-0) band of the IR atmospheric bands has been subject

to a wealth of VIRTIS limb observations so that the average behavior and the variability of this emission have been extensively described in the recent literature (Piccioni et al., 2009; Gérard et al., 2009; Soret et al., 2012). The mean hemispheric nightside area-weighted nadir intensity observed over the full period of VIRTIS-M operation is 0.5 MR.

The Herzberg II and Chamberlain bands are too weak to be measured at nadir. Therefore, only the limb intensities may be used to quantify the brightness of these two emissions. The Herzberg II bands have been characterized in terms of limb profiles and intensity with the VIRTIS instrument, as was previously described. The results by Migliorini et al. for the (0-7) to (0-11) bands must be combined with the transition probabilities calculated by Bates (1989) to obtain the total intensity of the (0-v'') progression for v'' = 0 to 14. The limb intensity of the Herzberg II emission in Table 1 represents the averaged value of the individual emission peaks of the seven limb profiles exhibiting all bands from (0-7) to (0-11) scaled with the appropriate factor of 1.47. This averaged total Herzberg II limb peak intensity is 149 kR, in close agreement with the earlier measurements by García-Muñoz et al. (2009). They obtained a peak brightness of 128 kR for the summed intensity for bands v'' = 6-11 bands in their average limb spectrum of the nightside, corresponding to 157 kR for all v'' levels. The new VIRTIS value leads to an IR Atm/HzII ratio of 188.

As mentioned before, the Chamberlain bands are considerably weaker and more difficult to observe than the other two band systems. The intensity determination from VIRTIS relies on only two limb profiles where the Chamberlain bands can be clearly distinguished from the Herzberg II bands. The corresponding peak brightness of 53 kR for the total peak Chamberlain system is obtained by multiplying the observed average peak value of 17.8 kR for the sum of the (0-6) and (0-7) bands by a factor of 3 corresponding to the branching ratio calculated by Bates (1989). The statistical error on

this value is estimated on the order of 30%. These values lead to an average Herzberg II/Chamberlain intensity ratio of 2.9. However, we consider this Chamberlain band intensity as overestimated since it refers to the only two positive detections among a much larger number of non-detections. Another estimate of the brightness of the Chamberlain bands was provided by Krasnopolsky (1983), based on the Venera observations. The intensity ratio of Herzberg II to the Chamberlain emission in the Venera observations was estimated equal to 13.4, a value considerably larger than the average ratio of 2.9 obtained from VIRTIS. We adopt this ratio for further discussion as it is based on a better signal statistics than the VIRTIS observations. We note that the Venera spectrometers did not measure the IR Atmospheric 1.27 m emission, so that its relative intensity to the Herzberg II and Chamberlain systems is derived from VIRTIS measurements.

3. Model calculations of the O_2 nightglow emissions

Following formation of an O_2 excited state in process (1), the molecules deactivate through spontaneous radiative transitions and collisional quenching by major constituents such as CO_2 and O:

$$O_2^* + X \rightarrow O_2 + X \qquad (2)$$

The identity of the quenching species X appears to play a major role in the control of the efficiency of the collisional deactivation and determines which systems are dominant in a given planetary atmosphere. In the case of the Venus nightside, the IR atmospheric bands are by far the most intense, followed by the Herzberg II, and the weak Chamberlain bands.

The Herzberg I, the Atmospheric and the Noxon bands have not been observed in the Venus nightglow.

3.1. Formulation

Some of the quenching coefficients have been measured in the laboratory, but several ones are not known or only upper limits have been determined. These coefficients and the radiative lifetimes of the a $^1\Delta$, c $^1\sum$ and the A' $^3\Delta$ metastable states have been recently reviewed by García-Muñoz et al. (2009) and Krasnopolsky (2011) on the basis of the available ground-based and space observations of the atmospheres of the three planets. As a starting point, we combine the existing laboratory values with those recommended by Krasnopolsky. The latter are adjusted when necessary to best match the altitude measurement by VIRTIS listed in Table 1 of the three O_2 emissions results.

The volume emission rate of the O_2 airglow emission from the metastable i state is given by

$$\eta_i(O_2,i) = \varepsilon_i K [O]^2 [M] \frac{A_i}{1/\tau_i + k^i_{CO_2}[CO_2] + k^i_O[O]} \quad (3)$$

where

[M] is the total number density , [O] and [CO_2] the local numbers densities of O and CO_2

$_i$ the net yield of the i state of O_2 , including contributions of cascades from upper states

A_i the Einstein spontaneous transition probability of the transition

$_i$ the radiative lifetime of the i state

K is total rate coefficient of processes (1)

k^i_{CO2} and k^i_O the quenching coefficients of the i state by CO_2 and O respectively

We note that the reaction coefficient for process (1) with N_2 as a third body was initially measured by Campbell and Trush (1967). A more recent measurement by Pejakovic et al. (2008) is close to the earlier value of 2.7×10^{-33} $cm^6 s^{-1}$ at 300 K. For consistency with the

value adopted by Soret et al. (2012) to derive the O density distribution from the 1.27 m airglow, we adopt a value of 2.5 times 1.25×10^{-32} $cm^6 s^{-1}$ at 185 K for CO_2 as the main third body. If the CO_2 and O density distributions are known, the volume emission of each transition may be calculated. Following integration along the line of sight, nadir intensity and emission limb profiles may be calculated and compared with the satellite observations. If discrepancies are observed, they may be used to correct and improve the quenching coefficient data sets. In the following, we describe the CO_2 and O mean nightside density vertical distribution adopted to model the O_2 nightglow emission profiles. As a starting point, we use a set of quantum yields based on a compilation of earlier measurements of the characteristics of the oxygen emissions in terrestrial atmospheres.

3. 2. Neutral densities and adopted coefficients

No direct in situ measurements of the CO_2 or O number densities have been made in the range of altitudes considered in this study so far. The measurements with the Orbiting Neutral Mass Spectrometer (ONMS) on board the Pioneer Venus orbiter were limited to low latitudes and altitudes above 145 km. Consequently, in the region of the oxygen airglow emissions, the VTS3 empirical model (Hedin et al., 1983), which is largely based on Pioneer Venus ONMS densities, only provides extrapolations of the measurements at higher altitudes based on the hydrostatic equilibrium assumption. This assumption is approximately valid for inert molecules such as CO_2 provided that the thermal vertical profile is known. However, for atomic oxygen which is subject to photochemical processes, this approximation fails and does not predict a density maximum in the vicinity of the mesosphere-thermosphere transition region. This is in contradiction with numerical simulations based on the three-dimensional Venus Thermospheric General Circulation Model (VTGCM, *Bougher et al.*, 1990),

which combines chemical, dynamical and energetic processes. Based on an updated version of the VTGCM, Brecht et al. (2011, 2012) predict the presence of an O density peak near 100 km. Nightside airglow limb observations with the VIRTIS multispectral infrared imager also indicate that the O_2 $a^1\Delta \rightarrow X\ ^3\sum$ emission at 1.27 m presents a peak near 96 km, an evidence for the presence of a maximum in the O density vertical distribution.

In order to root the model calculations into recent measurements, we have adopted density values derived from recent studies of airglow emissions and stellar occultations made with Venus Express remote sensing instruments. Figure 1 shows the adopted CO_2 and O density profiles. The carbon dioxide profile is derived from the analysis by Soret et al. (2012) of 114 observed CO_2 density profiles extracted from SPICAV stellar occultations (Montmessin et al., 2006) on the nightside. Soret et al. (2012) generated a three-dimensional statistical map of the CO_2 density from which the mean CO_2 density profile averaged over the Venus nightside is derived for these simulations. It is not drastically different from the VTS3 densities below 145 km. The oxygen density vertical distribution is the averaged profile of the three-dimensional statistical O density map obtained by Soret et al. (2012). This map is based on VIRTIS limb and nadir observations of the $O_2(a^1\Delta)$ nightglow at 1.27 m from which the O density distribution may be derived (Gérard et al., 2009a). The average O density nightside profile reaches a maximum of 1.9×10^{11} cm^{-3} at 103.5 km. This value is in close agreement with those obtained with the VTGCM reported by Brecht et al. (2012).

4. Results and sensitivity tests

The methodology adopted here is i) to start with the list of quenching coefficients and yields listed in Table 2, ii) calculate the associated limb profiles and the altitude differences between the emission peaks, iii) make the necessary adjustments to the quenching

coefficients which are not or loosely experimentally determined and iv) adjust the yields to obtain the best possible match with the observed intensity ratios.

Table 2 lists the yields and the quenching coefficients initially adopted, the calculated altitude of the peaks of the visible airglow layers, and their limb maximum intensity. The efficiency for the production the $a^1\Delta$ state is taken as 0.75 for consistency with the value adopted in the studies by Gérard et al. (2009a) and Soret et al. (2012) to determine the O density distribution from the 1.27 m airglow. Only an upper limit of $2x10^{-20}$ cm^{-3} s^{-1} has been determined for the quenching coefficient of the a $^1\Delta$ state by CO_2 (Sander et al., 2006). Following Krasnopolsky (2011), we adopt a value of $1x10^{-20}$ cm^{-3} s^{-1}, noting that using smaller values affects neither the peak intensity nor its altitude. This value was shown to be compatible with the observations of the O_2 Martian nightglow at 1.27 m by Gagné et al. (2012). The efficiency of the production of the c $^1\sum$ state is taken as 0.03 but it is left as a free parameter to be adjusted to fit the observed limb profile. The quenching coefficient of the c $^1\sum$ state by O is taken from the laboratory measurements by Kenner and Ogryzlo (1983), while the initial coefficient for CO_2 quenching is from Krasnopolsky (2011) and allowed to vary to provide the best fit. The A' $^3\Delta$ state is deactivated by O with k = $1.3x10^{-11}$ cm^{-3} s^{-1} (Kenner and Ogryzlo, 1983) and by CO_2 at an initial value of $4.5x10^{-13}$ cm^{-3} s^{-1}. The net production efficiency is taken equal to 0.12, as suggested by Krasnopolsky (2011). Finally, although the Herzberg I system has not been observed in the Venus nightglow, we calculate its emission profile using the parameters listed in Table 2. The purpose is to determine its expected limb intensity and discuss the absence of positive identification.

The comparison of the modeled values in columns (a) of Table 1 with the VIRTIS observations indicates that, as expected, the altitude of the maximum limb intensity of the IR Atmospheric emission is properly simulated. We also note that the model correctly predicts that the Chamberlain emission is at the highest altitude of all O_2 emissions and that the

Herzberg II bands occur significantly lower. The altitude of the maximum Chamberlain bands at 100 km is correctly predicted. The calculated Herzberg II peak intensity is located 0.8 km below the observed value of 95.3 km. We thus conclude that the initial set of quenching coefficients of the c state should be somewhat modified to better match the observations.

Figures 2 illustrates the distribution of the O_2 recombination rate and of the volume emission rates of the O_2 IR atmospheric, Herzberg I, Herzberg II and Chamberlain bands calculated with the revised set of coefficients listed in Table 2 (columns labeled b). These coefficients are obtained by adjusting the values of the yields of the c and A' states and the quenching coefficients of the c state by CO_2 and O and of the A' state by CO_2.

Figure 3 shows the calculated limb intensities as a function of the altitude of the tangent point, obtained by integrating the curves of Figure 2 along the line of sight. It also shows the mean limb profiles of the O_2 IR atmospheric, Herzberg II and Chamberlain bands derived from VIRTIS observations. For the O_2 IR Atmospheric bands, the full set of O_2 limb profiles described by Soret et al. (2012) is used to define a hemispherically averaged profile. For the Herzberg II bands, we average the seven limb profiles exhibiting all bands from (0-7) to (0-11) (Table 1 of Migliorini et al.) and apply the appropriate scaling factor to determine the average limb profile of the emission total system. In the case of the Chamberlain bands, the average of the only two usable profiles is shown. Consequently, the peak intensities of these limb profiles (the average of the mean profile) are different from those listed in Table 1 (the average of the peak values). The comparison confirms that the altitudes of the IR atmospheric, Herzberg II and Chamberlain emissions are correctly predicted by the model. However, as can be seen in Table 1, the calculated peak intensity of the O_2 IR Atmospheric and Herzberg II bands are underestimated by a factor close to 2. To facilitate the comparison of the altitude distributions, we have scaled the brightness of all model curves on the plot by

a factor of 2.1. This factor might be the consequence of calculating the total oxygen recombination profile using separately derived nightside averaged O and CO_2 density profiles, which may be different from the average of the $[O]^2$ x $[CO_2]$ product. We note that García-Muñoz et al. (2009) derived a somewhat higher O density profile using a 50% a state production efficiency, a CO_2 density profile from VTS3, and slightly different rate coefficients. As discussed before, the calculated HerzbergII/Chamberlain intensity ratio is in good agreement with the Venera observations, but lower than the VIRTIS ratio.

For the $a^1\Delta$ state, the quenching coefficient by CO_2 is close to the experimental upper limit. A sensitivity test indicates that if $k_{CO2}(a)$ is divided by 10, the altitude of the emission remains unaffected. Similarly, a change by an order of magnitude of $k_O(a)$ does not affect the altitude of the emission peak. The same test for the $A'\ ^3\Delta$ state shows that a decrease of $k_{CO2}(A')$ by a factor of 10 lowers the peak altitude by 1 km, while an increase by the same factor leaves the altitude invariant at 100 km. Quenching by O acts in the opposite direction: an increase by 10 move the layer downward by 1.0 km, while an 10-fold decrease leave the altitude unchanged. This different behavior of the O_2 excited states with respect to quenching will be discussed in the section 5.

As mentioned in section 1, Kenner and Ogryzlo (1983) measured a value of $5.9x10^{-12}$ cm^{-3} s^{-1} for the quenching coefficient of the $c\ ^1\sum$ state by atomic oxygen. Their value refers to the 0 vibrational level of the c state which appears to be the most densely populated. They also found that the quenching coefficient by CO_2 is less than $6x10^{-14}$ cm^{-3} s^{-1}. We thus consider the former as experimentally determined and we examine the altitude dependence of the HzII airglow emission with respect to the latter starting from a value of $1.2x10^{-16}$ cm^{-3} s^{-1}. We find that using a value 10 times larger moves the Herzberg II airglow layer upward by 1.5 km. By contrast, a 10 times less value decreases the altitude by 0.5 km. The best fit value of $k_{CO2}(c) = 3.1x10^{-16}$ cm^{-3} s^{-1} is adopted (Table 2, b). The altitude of the Chamberlain bands is

correctly predicted and we do not suggest to modify the measured values of $k_O(A')$ = 1.3 x 10^{-11} cm^{-3} s^{-1} (Table 2, b). The set of and $k_i(j)$ values providing the best agreement with the observations are listed in Table 2, b. The corresponding model limb profiles are shown in Figure 3. We note that the decreasing order of the IR atmospheric, Herzberg II and Chamberlain band intensity is in agreement with the ratios listed in Table 3. Tests have been conducted with different vertical distributions of the CO_2 and O density profiles. For example, the CO_2 density from VTS3 (Hedin et al., 1983) has been used instead of the values derived from the SPICAV occultations. The sensitivity to the O density profile has also been assessed by using the vertical distributions calculated with the 3-D model by Brecht et al. (2012). These tests indicate that, although the altitude of the maximum intensity of all emissions depends to some extent on the CO_2 and O densities, the relative distance between the peaks of the various emissions remains largely constant.

The sensitivity tests to the value of the quenching coefficients lead to some interesting conclusions. The intensity of the IR Atmospheric system only increases by 2% if the value of $k_{CO2}(a)$ is set to zero and by 15% if both $k_O(a)$ and $k_{CO2}(a)$ are null. This result, combined with the lack of sensitivity of the peak altitude, confirms that quenching of the a $^1\Delta$ state plays a negligible role in the control of the 1.27 m emission layer at and above the emission peak.

The intensity of the maximum of the simulated Hz II limb profile drops by 31% for a ten-fold increase of $k_{CO2}(c)$ and increases by 8% for a ten-fold decrease. The brightness of the Herzberg II layer is thus fairly insensitive to the values of the quenching coefficients within a change of two orders of magnitude with respect to the initial set of coefficients.

The Chamberlain bands only weakly respond to variations of the values of the $k_O(A')$ quenching coefficients: their peak value increases by 3% if $k_O(A')$ is divided by a factor of 10 and decreases by 19% for a 10-times increase. By contrast, a 10-fold increase of $k_{CO2}(A')$

leads to a brightness 10 times lower while a 10-fold decrease produces an enhancement by a factor 7.9, clearly indicating the importance of collisional deactivation of the A' $^3\Delta$ state by CO_2.

The location of the maximum emission rates relative to that of the recombination rate of O atoms may be easily understood by considering extreme cases of expression (3) where radiative relaxation or collisional quenching by O or CO_2 controls the effective loss rate. If the dominant term in the denominator is the Einstein coefficient, the volume emission rate is simply proportional to the $[O]^2$ x $[CO_2]$ product and the emission peaks at the same altitude as the recombination rate. As it was shown in Figure 2, this is the case of the $a^1\Delta$ state. If the denominator is dominated by the k_{CO2} x $[CO_2]$ term, is proportional to $[O]^2$ and the maximum is located above that of the $[O]^2$ x $[CO_2]$ product. This is the case of the Chamberlain bands whose maximum is indeed observed above that of the IR Atmospheric bands. The third case, where quenching by O dominates, corresponds to proportional to $[O]x[CO_2]$, which has a maximum at an altitude intermediate between that of the $[O]^2$ x $[CO_2]$ and $[O]^2$ products.

5. Discussion

Comparing the net yields of the upper levels of the three observed emissions in Table 2, we note that the efficiency of the $a^1\Delta$ state is intentionally fixed to its original value of 0.75 for consistency with the model previously used to derive the O density from the 1.27 m airglow distribution. The 2.6% net yield of the c state is slightly less than the value used by Krasnopolsky (2011) but larger than the 1.35% suggested by García-Muñoz. The difference stems from the absence of quenching by oxygen in the latter model. The 12% derived for the population of the A' state is unchanged from the

initial value, as suggested by Krasnopolsky. We note that the sum of the net yields is 0.94, close to but less than unity. The other 6% possibly correspond to other weaker non-identified transitions not accounted for in this study. These values may be compared with the relative rate of O atom association at 180 K by Wraight (1982), based on the potential energy curves of the different O_2 states. The yield for the a state is considerably higher than the direct quantum efficiency of 5% following O atom association (Huestis, 2002). The fraction of direct association leading to the A' state was predicted to be 0.12, a value providing good agreement with the effective fraction used to model the Venus Chamberlain bands. For the c state, Wraight (1982) derived a direct fraction of 0.04 compared to the 0.026 value based on the VIRTIS measurements.

Table 2 indicates that the quenching coefficient of the c state derived from the best match with the observations is 2.5 times larger than the initial value if the quenching coefficient by O measured in the laboratory is used. As expected, the efficiency and quenching of the a state are in agreement with the initial values which were based on the analysis of the 1.27 m IR Atmospheric emission. The yield and the quenching coefficient by CO_2 are in excellent agreement with the initial values listed in Table 2, with k_{CO2} slightly below the initial value.

Figures 2 and 3 also illustrate the predicted volume emission rate and limb profiles for the Herzberg I bands. The total system intensity is less than for the Chamberlain system. Abel numerical integration of this emission yields a limb intensity of 2.5 kR, that is about half of the Chamberlain band brightness. On the basis of the transition probabilities (Bates, 1989) and assuming that most of the population of the A state is in the v''=0 level, the strongest bands of the v'=0 progression are expected to lie between 400 and 530 nm. No statistical coincidence was found with the expected band positions analyzed in Migliorini et al. (submitted to Icarus). The presence of the weak

v′=0 progression in the Venera spectra was detected by Krasnopolsky (1983) with a vertical intensity for the total system of 140 R. The spectrally widespread nature of the Herzberg I bands, combined with the marginal signal to noise ratio of the VIRTIS visible nightglow spectra, possibly explains this lack of positive identification in the VIRTIS spectra. Future observations in the visible with higher spectral resolution and sensitivity should help clarifying this issue.

REFERENCES

Allen, D., Crisp, D., Meadows, V., 1992. Variable oxygen airglow on Venus as a probe of atmospheric dynamics, Nature, 359, 516.

Bailey, J., Meadows, V. S., Chamberlain, S., Crisp, D., 2008. The temperature of the Venus mesosphere from O_2 ($a^1\Delta_g$) airglow observations, Icarus, 197, 247-259.

Bates, D.R., Excitation and quenching of the oxygen bands in the nightglow, 1988. Planet. Space Sci., 36, 875-881.

Bates, D. R., 1989. Oxygen band system transition arrays, Planet. Space Sci., 37, 881– 887.

Bougher, S. W., Gérard, J. C., Stewart, A. I. F., Fesen C. G., 1990. The Venus nitric oxide night airglow: model calculations based on the Venus Thermospheric General Circulation Model, J. Geophys. Res., 95, 6271-6284.

Bougher, S. W., Borucki, W. J., 1994. Venus O_2 visible and IR nightglow: Implications for lower thermosphere dynamics and chemistry, J. Geophys. Res., 99, 3759– 3776.

Brecht, A. S., Bougher, S. W. Gérard, J.-C., Parkinson, C., Rafkin, S., Foster B.. 2011. Understanding the variability of nightside temperatures, NO UV and O_2 IR nightglow emissions in the Venus upper atmosphere, J. Geophys. Res., 116, E08004, doi:10.1029/2010JE003770.

Brecht, A. S., S. W. Bougher, J. C. Gérard, and L. Soret (2012), Atomic oxygen distributions in the Venus thermosphere: Comparisons between Venus Express observations and global model simulations, Icarus, 217, 2, 759-766.

Campbell I. M. , Thrush, B.A., 1967. Recombination of nitrogen atoms and nitrogen afterglow. Proc. R. Soc. Lond. A, 296, 201-221, 1967.

Connes, P., Noxon, J. F., Traub, W. A., Carleton, P., 1979. $O_2(^1\Delta)$ emission in the day and night airglow of Venus, Astrophys. J., 233, L29–L32.

Crisp, D., Meadows, V. S., Bézard, B., de Bergh, C. Maillard, J.-P., Mills, F. P., 1996. Ground-based near-infrared observations of the Venus nightside: 1.27-mm $O_2(a^1\Delta_g)$ airglow from the upper atmosphere, J. Geophys. Res., 101, 4577– 4593.

Drossart, P., et al., 2007. A dynamic upper atmosphere of Venus as revealed by VIRTIS on Venus Express, Nature 450, 641-645.

Gagné, M.-È., Melo, S. M. L., Lefèvre, F., González-Galindo, F., Strong., K., 2012. Modeled O_2 airglow distributions in the Martian atmosphere, J. Geophys. Res., 117, E06005, doi: 10.1029/2011JE003901.

García-Muñoz, A., Mills, F. P., Slanger, T. G., Piccioni, G., Drossart, P., 2009. Visible and near-infrared nightglow of molecular oxygen in the atmosphere of Venus, J. Geophys. Res., 114, E12002, doi:10.1029/2009JE003447.

Gérard, J. C., Saglam, A., Piccioni, G., Drossart, P., Cox, C., Erard, S., Hueso, R., Sanchez-Lavega, A., 2008. Distribution of the O_2 infrared nightglow observed with VIRTIS on board Venus Express, Geophys. Res. Lett. 35, L02207, doi:10.1029/2007GL032021.

Gérard, J.-C., Saglam, A. , Piccioni, G. , Drossart, P. , Montmessin, F. , Bertaux, J.-L., 2009a. Atomic oxygen distribution in the Venus mesosphere from observations of O_2 infrared airglow by VIRTIS-Venus Express, Icarus, 199, 264–272.

Gérard, J.-C., Cox, C., Soret, L., Saglam, A., Piccioni, Bertaux, J.-L., Drossart., P., 2009b. Concurrent observations of the ultraviolet nitric oxide and infrared O_2 nightglow emissions with Venus Express, J. Geophys Res., 114, E00B44.

Gérard, J.-C., Soret, L., Saglam, A., Piccioni, G., Drossart, P., 2010. The distributions of the OH Meinel and O_2 ($a^1\Delta$-$X^3\Sigma$) nightglow emissions in the Venus mesosphere based on VIRTIS observations, J. Adv. Space Res., 45, 1268-1275.

Hedin, A.E., Niemann, H.B., Kasprzak, W.T., Seiff, A., 1983. Global empirical model of the Venus thermosphere, J. Geophys. Res., 88, 73-83.

Huestis, D.L., 2002. Current laboratory experiments for planetary aeronomy, in Atmospheres in the Solar System – Comparative Aeronomy, M. Mendillo, A. Nagy, J.H. Waite, eds., AGU Monograph 130, 245–258.

Kenner, R. D., Ogryzlo, E. A., 1983. Quenching of $O_2(c\ ^1\Sigma+u, v=0)$ by $O(^3P)$, $O_2(a\ ^1\Delta g)$ and other gases, Can. J. Chem., 61, 921-926.

Krasnopolsky, V.A., 1983. Venus spectroscopy in the 3000–8000 A region by Veneras 9 and 10, in Hunten, D.M., Colin, L. Donahue, T.M. Moroz, V.I. (eds), Venus. University of Arizona Press, Tucson, AZ, 459-483.

Krasnopolsky, V.A., 2011. Excitation of the oxygen nightglow on the terrestrial planets, Planet. Space Sci., 59, 754-766.

Migliorini, A., Piccioni, G., Gérard, J.C., Soret, L., Slanger, T., Politi, R., Snels, M., Drossart, P., Nuccilli, F. The characteristics of the O_2 Herzberg II bands observed with VIRTIS/Venus Express, submitted to Icarus.

Lellouch, E., Clancy, T., Crisp, D., Kliore, A., Titov, D., Bougher, S.W. 1997. Monitoring of mesospheric structure and dynamics. In: Bougher, S.W., Hunten, D.M., Philips, R.J. (Eds), Venus II: Geology, Geophysics, Atmosphere, and Solar Wind Environment. Univ. of Arizona Press, Tucson, p. 295.

Montmessin, F., Quémerais, E., Bertaux, J. L. , Korablev, O., Rannou, P., Lebonnois, S., 2006. Stellar occultations at UV wavelengths by the SPICAM instrument: Retrieval and analysis of Martian haze profiles, J. Geophys. Res., 111, E09S09.

Ohtsuki, S., Iwagami, N., Sagawa, H. , Ueno, M. , Kasaba, Y. , Imamura, T. , Yanagisawa, K. , Nishihara, E., 2008. Distributions of the Venus 1.27- m O_2 airglow and rotational temperature, Planet. Space Sci., 56, 1391–1398.

Pejakovic, D.A., Kalogerakis, K. S., Copeland, R. A., Huestis, D.L., 2008. Laboratory determination of the rate coefficient for three-body recombination of oxygen atoms in nitrogen, J. Geophys. Res. 113, A04303, doi:10.1029/2007JA012694.

Piccioni, G., Zasova, L., Migliorini, A. , Drossart, P. , Shakun, A. , García-Muñoz, A. , Mills, F. P., Cardesin-Moinelo, A., 2009. Near-IR oxygen nightglow observed by VIRTIS in the Venus upper atmosphere, J. Geophys. Res., 114, E00B38, doi:10.1029.

Sander, S. P., et al. (2006), Chemical kinetics and photochemical data for use in atmospheric studies, NASA Eval. 15, Jet Propul. Lab., Pasadena, California.

Slanger, T. G., Black, G., 1978. The $O_2(C^3\Delta_u \rightarrow a^1\Delta_g)$ bands in the nightglow spectrum of Venus, Geophys. Res. Lett, 5, 947–948.

Slanger, T. G., Copeland, R. A., 2003. Energetic oxygen in the upper atmosphere and the laboratory, Chem. Rev., 103, 4731– 4765.

Slanger, T. G., Huestis, D. L. , Cosby, P. C. , Chanover, N. J. , Bida, T. A., 2006. The Venus nightglow: Ground-based observations and chemical mechanisms, Icarus, 182, 1–9.

Soret, L., Gérard, J.C., Montmessin, F., Piccioni, G., Drossart, P., Bertaux, J.L., 2012. Atomic oxygen on the venus nightside: Global distribution deduced from airglow mapping. Icarus, 217, 849-855.

Wraight,, P.C., 1982. Association of atomic oxygen and airglow excitation mechanisms, Planet. Space Sci., 30, 251–259.

Table 1: mean intensity and peak altitude of O_2 airglow emissions observed at the limb with VIRTIS and comparison with values calculated in this work.

Emission	VIRTIS observed mean intensity	altitude	calculated[a] intensity	altitude	calculated[b] intensity	altitude
IR atmospheric	28 MR	96.2 km	13 MR	96.0	13 MR	96.0
Herzberg II	149 kR	95.3 km	91 kR	94.5	70 kR	95.5
Chamberlain	53 kR	100 km	5 kR	100.0	5 kR	100.0
Herzberg I	not observed		3 kR	100.0	3 kR	100.0

[a]Based on the initial set of quenching coefficients (see Table 2)

[b]Calculated with modified set of quenching coefficient

Table 2: (a) list of initial efficiencies and quenching coefficients (cm^{-3} s^{-1}) of the upper states of the O_2 airglow transitions; (b) set of yields and quenching coefficients suggested in this work.

Emission	net yield		k_{CO2}		k_O	
	a	b	a	b	a	b
IR atmospheric	0.75	0.75	$1x10^{-20}$	$1x10^{-20}$	$2x10^{-16}$	$2x10^{-16}$
Herzberg II	0.03	0.026	$1.2x10^{-16}$	$3.1x10^{-16}$	$5.9x10^{-12}$	$5.9x10^{-12}$
Chamberlain	0.12	0.12	$4.5x10^{-13}$	$3.9x10^{-13}$	$1.3x10^{-11}$	$1.3x10^{-11}$
Herzberg I	0.04	-	$8x10^{-12}$	-	$1.3x10^{-11}$	-

Table 3: Comparison between observed and predicted relative intensities of visible nightglow features using values from Table 1, b and coefficients from Table 2, b .

Ratio	VIRTIS	Venera	Model
I(IR)/I(HzII)	188	153	185
I(HzII)/(Ch)	2.8*	13.5	13.5
I(HzII)/(HzI)	-	-	28.2

**Values based on two limb profiles.*

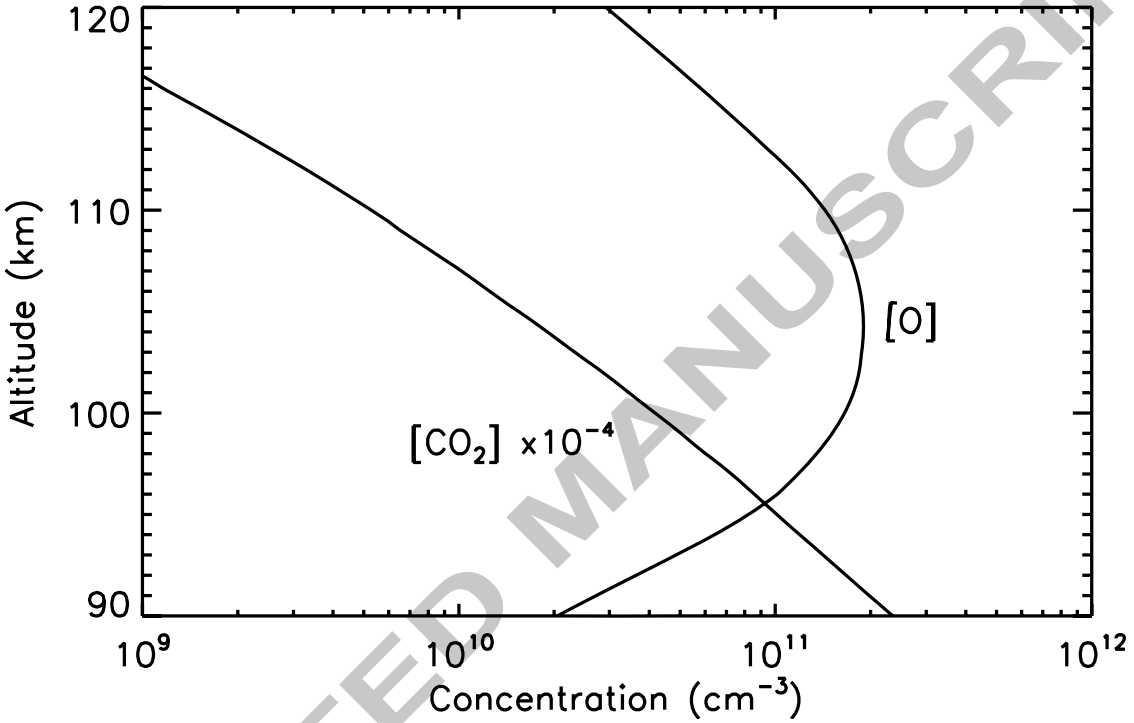

Figure 1: Average nightside O and CO_2 density profiles used in the visible airglow simulations. The O density is derived from the global oxygen model based on O_2 $^1\Delta$ nightglow observed with VIRTIS-M. The CO_2 density distribution is deduced from stellar occultations on the Venus nightside with the SPICAV instrument (Soret et al., 2012).

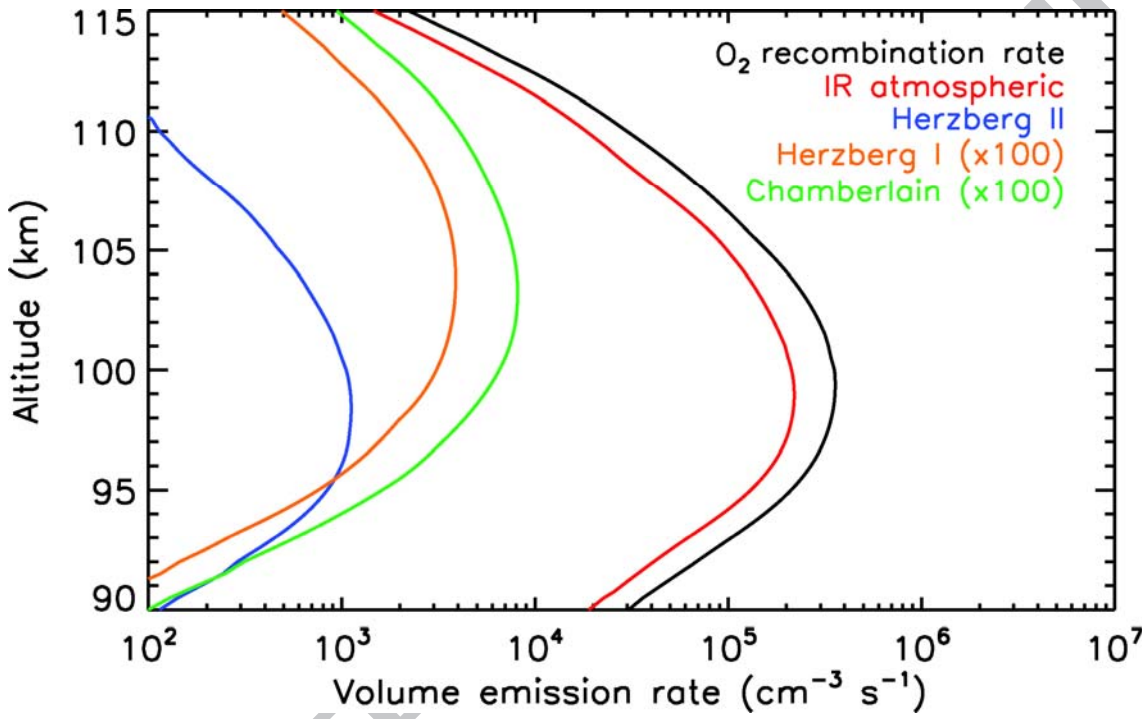

Figure 2: modeled volume emission rate profiles of the visible and infrared O_2 nightside airglow emissions using formula (1) and the set of yields and quenching coefficients listed in Table 2, columns b.

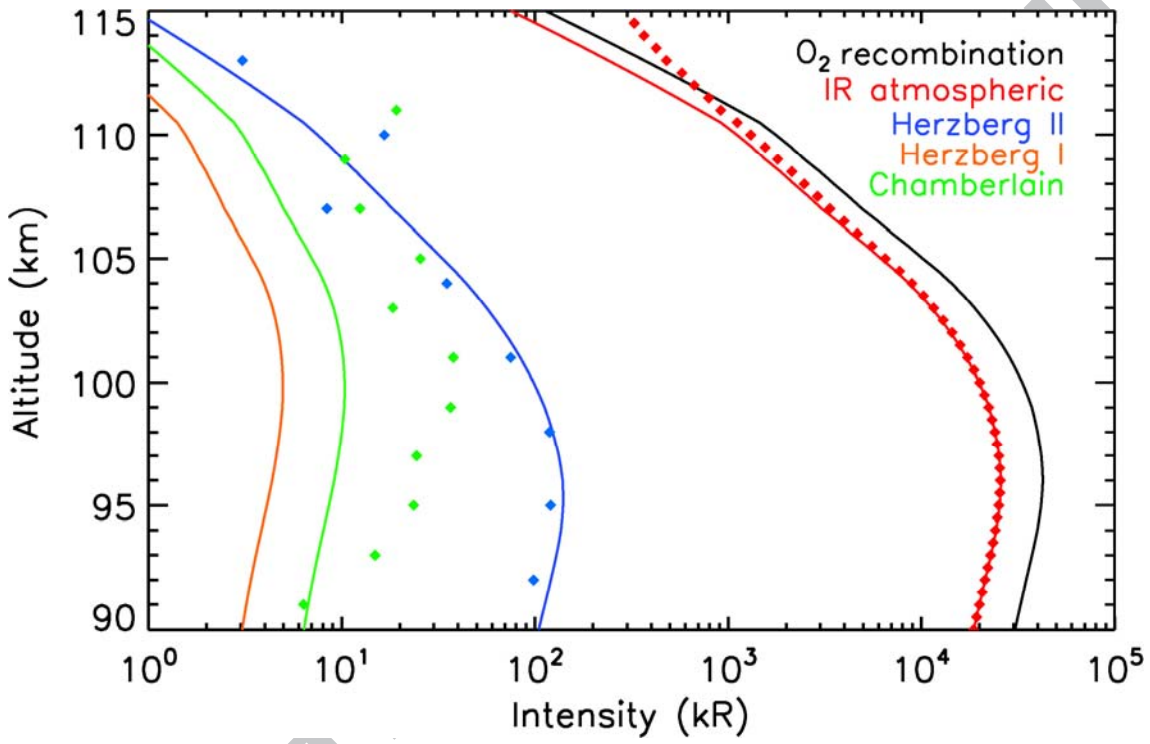

Figure 3: Modeled limb profiles of the O_2 nightside airglow obtained by integration along the line of sight of the volume emission rate shown in figure 2 (solid lines). The total O_2 recombination rate integrated along the line of sight is shown by the black solid line. For comparison, the average of the airglow limb profiles observed with VIRTIS-M and corrected for the total system intensities are also plotted (diamonds). The model curves have been scaled up by a factor of 2.1. The Chamberlain II bands intensities (green diamonds) observed with VIRTIS are based on two profiles only and are not considered as representative of the

actual mean intensity. The Chamberlain I bands have not been observed so far in the Venus nightglow.

Paper highlights

- Visible and near infrared O_2 emissions on the Venus nightside are modeled
- Differences in peak altitudes are interpreted in terms of collisional deactivation
- We predict higher altitude of the Chamberlain emission than the Herzberg II bands
- We compare with limb observations from VIRTIS onboard Venus express
- We derive values for yields of O_2 molecules and collisional quenching coefficients